Applicability of Metal/Insulator/Metal (MIM) Diodes to Solar Rectennas

Sachit Grover, *Student Member, IEEE*, and Garret Moddel, *Senior Member, IEEE*

***Abstract*—The current–voltage (*I–V*) characteristics of metal/insulator/metal (MIM) diodes illuminated at optical frequencies are modeled using a semiclassical approach that accounts for the photon energy of the radiation. Instead of classical small-signal rectification, in which a continuous span of the dc *I–V* curve is sampled during rectification, at optical frequencies, the radiation samples the dc *I–V* curve at discrete voltage steps separated by the photon energy (divided by the electronic charge). As a result, the diode resistance and responsivity differ from their classical values. At optical frequencies, a diode with even a moderate forward-to-reverse current asymmetry exhibits high quantum efficiency. An analysis is carried out to determine the requirements imposed by the operating frequency on the circuit parameters of antenna-coupled diode rectifiers, which are also called rectennas. Diodes with low resistance and capacitance are required for the *RC* time constant of the rectenna to be smaller than the reciprocal of the operating frequency and to couple energy efficiently from the antenna. Existing MIM diodes do not meet the requirements to operate efficiently at visible-to-near-infrared wavelengths.**

***Index Terms*—Metal/insulator/metal (MIM) diode, optical rectenna, photon-assisted tunneling, photovoltaics, rectenna, solar cell.**

I. Introduction

THE search for an efficient and low-cost solar cell has led to a resurgence of interest in energy conversion through rectification of solar radiation [1], [2]. This idea was originally proposed by Bailey [3], and the first patent on solar rectification was issued to Marks [4]. A rectenna is formed from an antenna and a diode connected as shown in Fig. 1. Rectennas, which is short for a rectifying antenna-coupled diode, operate by converting incident electromagnetic radiation into an ac electric field via the antenna, channeling this field across the diode, and rectifying the ac to provide dc power. This device can be configured as an energy converter or as a detector [5]. Significant research was conducted in the 1960s and 1970s toward the use of rectennas for microwave-powered helicopters and airplanes [6]. Conversion of energy from microwave to dc using rectennas has progressed from concept to application [7] and single-frequency conversion efficiency greater than 90% [8] has been demonstrated. By comparison, the technology for rectification of infrared and visible radiation is still in its infancy.

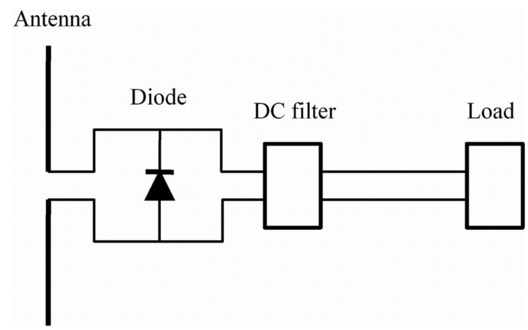

Fig. 1. Schematic of an antenna-coupled diode rectifier, which is also known as a rectenna.

Several fundamental and technological challenges arise when the operation of a rectenna is extended to ultrahigh (visible) frequencies ($\sim 10^{15}$ Hz). Scaling the rectenna from microwave to visible requires antennas with submicrometer dimensions. A possible technique for fabricating small antennas over a large area has been recently demonstrated [9]. An even bigger challenge is developing a diode that can operate efficiently at petahertz. Schottky diodes are frequency limited to the far-infrared [7], [10], [11]. A candidate of current interest is the metal/insulator/metal (MIM) tunnel diode [12]–[17], in which the nonlinearity is based on the femtosecond fast transport mechanism of quantum tunneling [18], [19]. MIM diodes have been successfully demonstrated for use in detectors operating at gigahertz [20], but the efficiency of MIM-based rectennas has been limited at higher frequencies [21], [22], [12]. To date, we are not aware of any experimental evidence for direct solar rectification using MIM-diode rectennas.

Sarehraz *et al.* [23] identify two difficulties that impede the performance of rectennas at high frequency. First, in the infrared and visible, metals are no longer perfect conductors, which leads to resistive losses in the antenna [24]. Second, the efficiency of power conversion from ac to dc depends on the power incident on a rectenna, which is small for a submicrometer scale antenna. Even if we assume that the first issue can be resolved using dielectric antennas [25], and the second shortcoming can be overcome by using concentrators, there is a more basic problem at hand. A rectenna operating at petahertz must have a low *RC* time constant and must efficiently transfer power from the

Manuscript received March 16, 2011; revised June 7, 2011; accepted June 13, 2011. Date of publication September 19, 2011; date of current version October 27, 2011.

S. Grover was with the Department of Electrical, Computer, and Energy Engineering, University of Colorado at Boulder, Boulder, CO 80309-0425 USA. He is now with the National Renewable Energy Laboratory, Golden, CO 80401 USA (e-mail: sachitgrover@ieee.org).

G. Moddel is with the Department of Electrical, Computer, and Energy Engineering, University of Colorado at Boulder, Boulder, CO 80309-0425 USA (e-mail: moddel@colorado.edu).

Color versions of one or more of the figures in this paper are available online at http://ieeexplore.ieee.org.

Digital Object Identifier 10.1109/JPHOTOV.2011.2160489

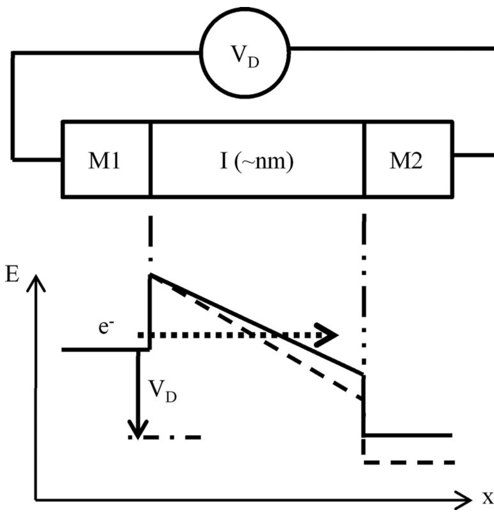

Fig. 2. Energy-band diagram of a single-insulator MIM diode. Change in applied voltage linearly changes the tunnel distance. The tunnel current depends exponentially on this distance, leading to nonlinear *I–V* characteristics.

antenna to the diode, requiring these elements to be impedance matched. As we show in this paper, for MIM diodes, these requirements conflict with each other for visible-light frequencies and are relaxed as the wavelength increases into the infrared.

In Section II, we describe the MIM diode, its principle of operation, and its performance metrics. At infrared and visible-light frequencies, the diode metrics and the current–voltage (*I–V*) curve under illumination need to be derived from a semiclassical analysis, as summarized in Section III. The deviation of the diode properties from their classical values is also explained. In Section IV, we analyze the tradeoffs in designing a rectenna solar cell. We emphasize the significance of the antenna impedance in the diode coupling efficiency.

II. Metal/Insulator/Metal Diodes

An MIM diode incorporates an insulator that is a few nanometers thick between two metal electrodes. The energy-band profile of such a diode is shown in Fig. 2. The probability of an electron tunneling across the insulator depends exponentially on the distance it has to traverse while in the bandgap of the insulator. Since this distance changes linearly with the diode voltage for an appropriate set of diode parameters (barrier heights, thickness, and voltage), the current is an exponential function of the voltage [26].

Earlier versions of MIM diodes, called cat-whisker diodes, were made from a thin wire pressed against a sheet of oxidized metal. This technique produced small-area diodes without submicrometer lithography and enabled the experimental demonstration of infrared detection and mixing using MIM diodes [27] at the expense of limited reproducibility, reliability, and stability. Recently, improved lithographic resolution has made feasible the fabrication of small-area diodes using thin-film metals and insulators with improved designs and material choices [12]. Deposited metal electrodes and insulators [16], [20], [28] allow well-controlled layer thicknesses and uniform interfaces. Despite the choice of materials that can be deposited by sputtering or evaporation, arbitrary combinations of metals and oxides are not feasible due to the formation of interfacial compounds. Such an unintended interfacial layer is evident in the TEM cross section of the ZrCuAlNi–Al_2O_3 interface [28], which could provide the advantages of a double-insulator diode described later.

To make an efficient rectenna, the MIM diode needs to have several characteristics. One is high responsivity, which is a measure of the rectified dc voltage or current as a function of input radiant power. This can be calculated directly from the diode *I–V* characteristics. The current responsivity is given by the ratio of the second and first derivatives of current with respect to voltage [29]:

$$\beta = \frac{1}{2}\frac{I''}{I'}. \tag{1}$$

Another characteristic is low resistance, of the order of 100 Ω, to provide good impedance matching between the antenna and the diode. A third property of the diode that is linked to the responsivity and is important for solar rectennas is the asymmetry in the *I–V* curve. Since it is desirable to operate the rectenna without applying an external dc bias, the diode must have asymmetric characteristics.

In designing MIM diodes, there is a tradeoff between these characteristics. An MIM diode can have asymmetric *I–V* if different metals are used on the two sides of the insulator, giving unequal barrier heights [30]. High barrier asymmetric diodes provide a large responsivity [31]. However, keeping the diode resistance low requires low barrier heights on both sides, which limits the asymmetry [12]. To achieve a high responsivity, requiring substantial nonlinearity while maintaining low resistance, one can resort to a multi-insulator tunnel barrier.

There are two mechanisms that allow multi-insulator diodes to have a high nonlinearity while keeping the resistance low [32]. Here, we describe their operation for tunnel barriers comprising two insulators having unequal barrier heights. One of the mechanisms makes use of resonant tunneling of electrons through a quantum well formed between the two insulators [12], [33]. This occurs when the metal Fermi level on the higher barrier side is biased positive creating a right-triangular well at the interface of the two insulators. When an allowed energy level in the quantum well aligns with the metal Fermi level on the negative side, it causes a sharp turn-ON of the diode. In the other mechanism, which occurs for the opposite bias polarity, an abrupt increase in current occurs when the metal Fermi level on the higher barrier side rises above the conduction band of the lower barrier, thereby decreasing the tunnel distance [34]. In a particular diode, the choice of insulator materials and thicknesses determines the mechanism that dominates.

III. Illuminated Diode Characteristics

Only at a relatively low (below a few terahertz, depending on the diode) frequency can a tunnel diode be considered as a classical rectifier [12]. When the voltage corresponding to the energy of the incident photons ($E_{\mathrm{ph}}/e = \hbar\,\omega/e$) is comparable with or greater than the voltage scale over which curvature in the diode's *I–V* curve is significant, a semiclassical analysis

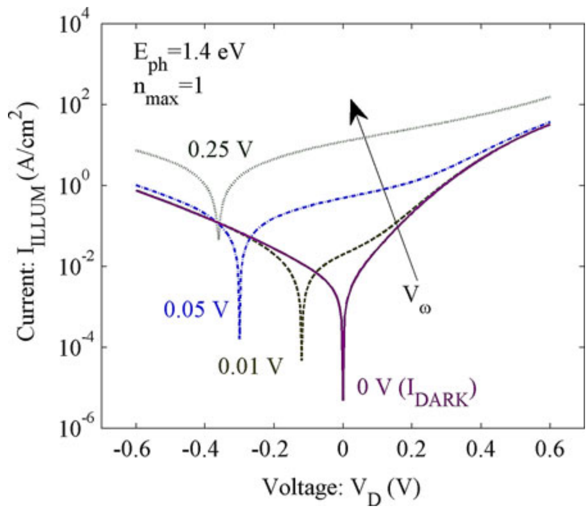

Fig. 3. Calculated *I–V* characteristics under various levels of excitation for a Nb/Nb$_2$O$_5$(3 nm)/Ta$_2$O$_5$(1.75 nm)/NbN MIIM diode. The $I_{\rm DARK}$ is the experimentally determined *I–V* for the diode. The other curves are simulated based on $I_{\rm DARK}$ and show the open-circuit voltage and short-circuit current increasing with increased ac signal V_ω. The ratio of $eV_\omega/E_{\rm ph}$ is small, allowing a first-order approximation of (2) to be used.

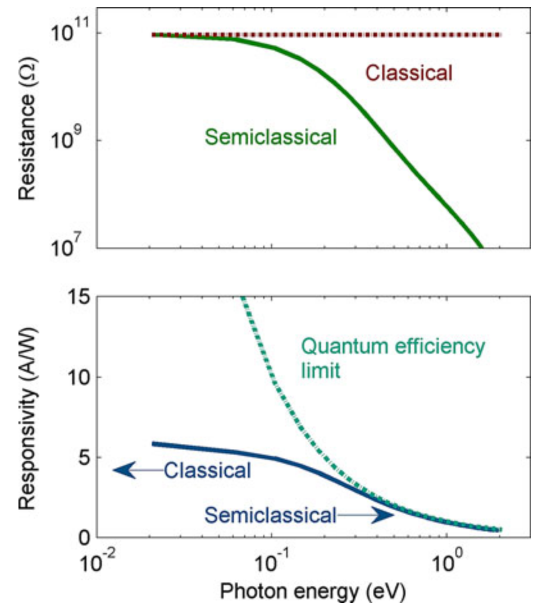

Fig. 4. Resistance and responsivity versus photon energy calculated classically and semiclassically using the finite difference forms given by (3a) and (3b) for the diode of Fig. 3, with $V_D = 0$ V. At high photon energy, the semiclassical resistance is significantly lower than the classical value, and the semiclassical responsivity approaches that for unity quantum efficiency.

for the photon-assisted tunneling is required [35], [36]. From this analysis, we obtain the *I–V* relation for a diode under illumination ($I_{\rm ILLUM}$), which depends on the unilluminated *I–V* ($I_{\rm DARK}$), as given by

$$I_{\rm ILLUM}(V_D, V_\omega) = \sum_{n=-\infty}^{\infty} J_n^2(\alpha) I_{\rm DARK}\left(V_D + n\frac{E_{\rm ph}}{e}\right). \quad (2)$$

Here, J refers to the Bessel function, and V_ω is the amplitude of the ac signal applied across the diode at a radial frequency ω. We assume a constant V_ω to keep the analysis simple. Under constant illumination, V_ω varies with diode resistance and, therefore, with the dc bias. For $eV_\omega/E_{\rm ph} << 1$, the summation can be approximated by terms up to first order ($n = -1, 0, 1$).

The $I_{\rm ILLUM}$ versus voltage relation for an MIM diode determines in which *I–V* quadrant the rectenna provides power. Unlike conventional semiconductor junction solar cells, which operate in the fourth quadrant, rectennas operate as solar cells in the second. Equation (2) is applied to the experimentally measured dark *I–V* curve for an Nb/Nb$_2$O$_5$(3 nm)/Ta$_2$O$_5$(1.75 nm)/NbN double-insulator diode as shown in Fig. 3. This diode has a high forward-to-reverse current ratio, which is required to obtain a significant short-circuit current or open-circuit voltage. $I_{\rm ILLUM}$ versus voltage curves are plotted for four different values of V_ω, with $V_\omega = 0$ corresponding to the unilluminated *I–V*. As V_ω increases, corresponding to an increasing number of photons incident on a diode, the zero crossing of the illuminated *I–V* shifts leftward. This shows that as the power incident on the diode increases, a higher operating voltage and, thus, a greater efficiency can be achieved by the rectenna.

In the case of large $E_{\rm ph}$, the diode resistance R_D and responsivity β_i, calculated using the semiclassical analysis, take on the finite difference form given by (3a) and (3b) [29], shown at the bottom of the page. We introduce a semiclassical resistance for such *I–V* curves, which is the reciprocal of the slope of the secant between the currents at $V_D \pm E_{\rm ph}/e$, instead of the usual tangent at V_D for the classical case. The semiclassical responsivity reflects the change in the slope of the secant, rather than the continuous derivatives for the classical case given in (1). In the limit of $E_{\rm ph}/e \to 0$, these finite difference forms give the same values as the classical results. In Fig. 4, we plot the semiclassical resistance and responsivity at zero bias versus the photon energy $E_{\rm ph}$ for the MIIM diode using the $I_{\rm DARK}(V)$ shown in Fig. 3. As the photon energy increases, the resistance of the diode decreases and the responsivity decreases. At high $E_{\rm ph}$, the responsivity approaches the limit of $e/E_{\rm ph}$, which is the maximum achievable responsivity corresponding to a quantum efficiency of 1. Therefore, even a diode with poor quantum efficiency at low $E_{\rm ph}$ becomes more efficient and, thus, adequate at high $E_{\rm ph}$.

$$R_D = \frac{1}{I'} \to \frac{2(E_{\rm ph}/e)}{I_{\rm DARK}(V_D + (E_{\rm ph}/e) - I_{\rm DARK}(V_D - (E_{\rm ph}/e)} \quad (3a)$$

$$\beta_i = \frac{1}{2}\frac{I''}{I'} \to \frac{e}{E_{\rm ph}}\left[\frac{I_{\rm DARK}(V_D + (E_{\rm ph}/e) - 2I_{\rm DARK}(V_D) + I_{\rm DARK}(V_D - (E_{\rm ph}/e)}{I_{\rm DARK}(V_D + (E_{\rm ph}/e) - I_{\rm DARK}(V_D - (E_{\rm ph}/e)}\right]. \quad (3b)$$

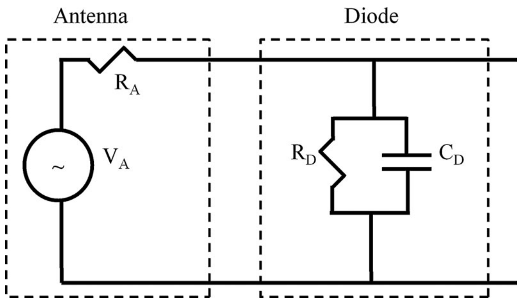

Fig. 5. Small-signal circuit model of the rectenna for determining coupling efficiency. The antenna is modeled as a voltage source in series with a resistance and the MIM diode is modeled as a resistor in parallel with a capacitor. Efficienct operation of the circuit requires matching R_A with R_D and keeping the time constant $(R_A \| R_D)C_D$ below the time period of the ac source V_A.

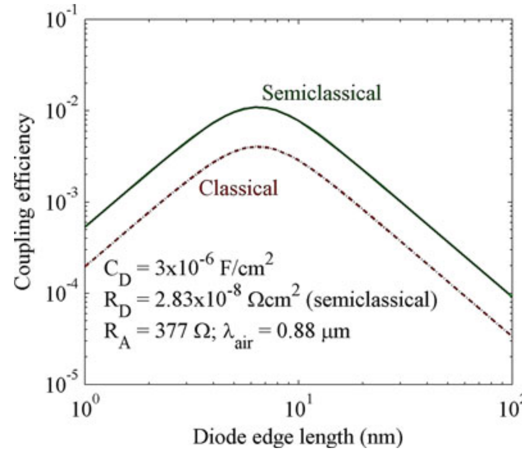

Fig. 6. Effect of varying the diode size on the antenna to diode coupling efficiency. The peak in the efficiency occurs due to the tradeoff between impedance match and cutoff frequency. The resistance of the Ni–NiO(1.5 nm)–Ni diode is calculated from its simulated *I–V* curve using the classical and the semiclassical ($E_{\mathrm{ph}} = 1.4$ eV, $\lambda_{\mathrm{air}} = 0.88\,\mu$m) forms of (3a). A Ni–NiO barrier height of 0.2 eV is used in the simulation [40].

IV. Antenna to Diode Coupling Efficiency

The thermodynamic cap on the efficiency of a rectenna solar cell is given by the Landsberg efficiency [37] limit of 93%. Several factors limit the experimentally achievable efficiency, including antenna radiation efficiency, resistive losses in the antenna, antenna-to-diode power transfer, and diode efficiency in converting ac to dc. Here, we examine the power transfer between the antenna and the diode, which is a function of the impedances of the two elements. This factor turns out to significantly limit the conversion efficiency for MIM-diode solar rectannas at optical frequencies.

In Section II, we mentioned the necessity for having low-resistance diodes that can be matched to the antenna, which is only the first constraint. The second is due to the *RC* time constant of the rectenna as obtained from the small-signal circuit shown in Fig. 5. The product of the antenna resistance R_A in parallel with the diode resistance R_D and the diode capacitance C_D must be smaller than the time period ($2\pi/\omega$) of radiation incident on the rectenna so that the antenna signal drops across the diode resistor R_D and is not shorted out by C_D.

Circuit analysis [12], [21] gives the overall efficiency of the rectenna to be proportional to the square of the coupling efficiency, which is the ratio of the ac power delivered to the diode resistance to the power of the antenna voltage source:

$$\eta_{\mathrm{coupling}} = \frac{P_{\mathrm{AC},R_D}}{P_{V_A}} = \frac{4(R_A R_D/(R_A + R_D)^2)}{1 + (\omega(R_A R_D/(R_A + R_D)C_D)^2}. \tag{4}$$

The conditions of $R_D = R_A$ and $\omega(R_A \| R_D)C_D << 1$ lead to a unity coupling efficiency, as can be seen from (4). The parameters that can be varied to achieve these conditions are the diode area, the antenna resistance, and the composition of the diode. The MIIM diode used in Section III is highly asymmetric but has a large resistance. A less-resistive diode will give a higher η_{coupling}. Therefore, for this analysis, we choose the Ni/NiO(1.5 nm)/Ni MIM diode, which has an extremely low resistance at zero bias and was used in several high-frequency rectennas [38]–[40]. Here, we are disregarding the fact that low-resistance and/or symmetric single-insulator diodes generally have a poor responsivity at zero bias [32].

Typical antenna impedances are of the order of 100 Ω [38]. We choose a nominal antenna impedance of 377 Ω, but as will become apparent, a different impedance would not help. We vary the diode area, which changes the diode resistance and capacitance. In Fig. 6, we show the η_{coupling} versus the diode edge length for a classically and semiclassically calculated diode resistance. The semiclassical resistance is lower than the classical resistance and gives a higher η_{coupling}. The peak in both the curves occurs at the same edge length and is an outcome of the balance between the needs for impedance matching and low cutoff frequency.

To understand the coupling efficiency better, one can separate the effects of impedance matching given by the numerator (ideally $R_D/R_A = 1$) and cutoff frequency given by the denominator (ideally $\omega(R_A \| R_D)C_D = 0$) in (4). Unity coupling efficiency under these conditions occurs for different edge lengths, as shown in Fig. 7(a). The overall efficiency is given by the smaller of the two values, limited by the two curves in Fig. 7(a), leading to the peak in Fig. 6. Increasing the diode resistance by a factor of 10 lowers the coupling efficiency by the same factor.

The tradeoff between impedance match to the antenna, for which a small R_D is desired, and a high cutoff frequency, for which a small C_D is desired, is fundamental for parallel plate devices. Varying the antenna impedance results in a simple translation of both curves in tandem such that the diode edge length for peak efficiency changes. With an increase in antenna impedance, a higher R_D can be accommodated, allowing the diode area to be smaller, and resulting in a desirable smaller C_D. However, the higher R_A also increases the $(R_A \| R_D)C_D$ time constant. This is shown in Fig. 7(b), where the higher antenna resistance shifts both curves to the left with no improvement in the coupling efficiency. In other words, to improve the coupling efficiency, the parameters in (4) would need to be adjusted so that the $\omega R_P C_D$ curve shifts to the right and the R_D/R_A curve shifts to the left.

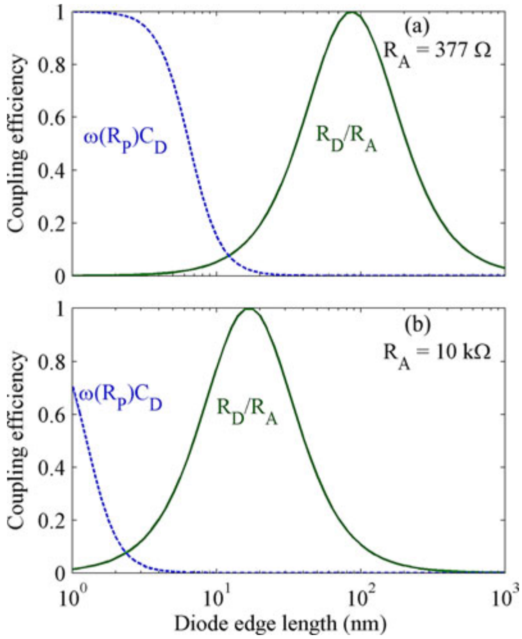

Fig. 7. Antenna-to-diode coupling efficiency as a function of diode edge length, separating the effect of impedance match from cutoff frequency for two antenna impedance values: (a) $R_A = 377\ \Omega$ and (b) $R_A = 10\ \mathrm{k}\Omega$. R_P denotes the parallel combination of R_A and R_D. The curves labeled $\omega R_P C_D$ show the coupling efficiency when only the cutoff frequency is the limiting factor, and those labeled R_D/R_A show the coupling efficiency when only the impedance match is the limiting factor. The maximum efficiency occurs for an edge length at the small peak where the two curves coincide.

The condition under which the constraints simultaneously lead to a high coupling efficiency is obtained by combining

$$\omega(R_A||R_D)C_D << 1 \text{ and } \frac{R_D}{R_A} = 1 \Rightarrow R_D C_D << \frac{2}{\omega}. \quad (5)$$

For the model Ni–NiO–Ni diode discussed earlier, this condition is not satisfied for near-infrared-light frequencies ($\lambda = 0.88\ \mu$m), where $2/\omega = 9.4 \times 10^{-16}$ s is much smaller than $R_D C_D = 8.5 \times 10^{-14}$ s. It is satisfied for wavelengths greater than 80 μm.

The time constant $R_D C_D$ is independent of the diode area and is determined solely by the composition of the MIM diode. As already noted, the Ni/NiO/Ni diode is an extremely low resistance diode, and NiO has a small relative dielectric constant ε_r of 10. Even if one could substitute the oxide with a material having comparable resistance and lower capacitance (best case of $\varepsilon_r = 1$), the $R_D C_D$ would still be too large for visible frequencies. A best case of $\varepsilon_r = 1$ occurs in Al_2O_3 near 30 THz [31], with the corresponding $R_D C_D = 20$ fs and $2/\omega = 100$ fs implying efficient coupling at that frequency. Putting practicality aside completely, a near-ideal resistance would result from a breakdown-level current density of 10^7 A/cm^2 at, say, 0.1 V, giving a resistance of $10^{-8}\ \Omega\cdot$cm^2. A near-ideal capacitance would result from a vacuum dielectric separated by a relatively large 10 nm, giving a capacitance of $\sim 10^{-7}$ F/cm^2. The resulting $R_D C_D$ would be $\sim 10^{-15}$ s, which, again is too large for efficient coupling at visible wavelengths.

The coupling efficiency of MIM-diode rectennas can be improved under certain circumstances. They become efficient at longer wavelengths, where the condition imposed by (5) is easier to meet. The $R_D C_D$ can also be artificially reduced by compensating the capacitance of the MIM diode with an inductive element, but this is difficult to achieve over a broad spectrum. A design that can circumvent the restrictions imposed on the coupling efficiency is the MIM traveling-wave rectifier [22], [41]. Akin to a transmission line where the geometry determines the impedance, the distributed *RC* enhances the coupling between the antenna and the traveling-wave structure. However, losses in the metallic regions of the waveguide limit its efficiency as the frequency approaches that of visible light.

V. Conclusion

The applicability of rectennas for solar energy harvesting rests on achieving efficient coupling between the antenna and the diode. Even though the tunneling process is femtosecond fast, MIM tunnel diodes are frequency limited due to their large *RC* time constant. In searching for a diode suitable for solar rectification, in addition to high speed and responsivity, the goal must be a device that has a combination of lower resistance and lower capacitance than the existing MIM diodes.

References

[1] R. Corkish, M. A. Green, and T. Puzzer, “Solar energy collection by antennas,” *Solar Energy*, vol. 73, no. 6, pp. 395–401, 2002.
[2] D. Y. Goswami, S. Vijayaraghavan, S. Lu, and G. Tamm, “New and emerging developments in solar energy,” *Solar Energy*, vol. 76, no. 1–3, pp. 33–43, 2004.
[3] R. L. Bailey, “A proposed new concept for a solar-energy converter,” *J. Eng. Power*, vol. 94, pp. 73–77, 1972.
[4] A. M. Marks, “Device for conversion of light power to electric power,” U.S. Patent 4 445 050, 1984.
[5] B. M. Kale, “Electron tunneling devices in optics,” *Opt. Eng.*, vol. 24, no. 2, pp. 267–274, 1985.
[6] W. C. Brown, “The history of power transmission by radio waves,” *IEEE Trans. Microw. Theory Tech.*, vol. MTT-32, no. 9, pp. 1230–1242, Sep. 1984.
[7] B. H. Strassner and K. Chang, “Rectifying antennas (rectennas),” in *Encyclopedia of RF and Microwave Engineering*. Hoboken, NJ: Wiley, 2005, p. 4418.
[8] W. C. Brown, “Optimization of the efficiency and other properties of the rectenna element,” in *Proc. IEEE-MTT-S Int. Microw. Symp.*, 1976, pp. 142–144.
[9] D. K. Kotter, S. D. Novack, W. D. Slafer, and P. Pinhero, “Solar nantenna electromagnetic collectors,” in *Proc. ASME Conf.*, 2008, vol. 2008, no. 43208, pp. 409–415.
[10] E. R. Brown, “A system-level analysis of Schottky diodes for incoherent THz imaging arrays,” *Solid-State Electron.*, vol. 48, pp. 2051–2053, Mar. 2004.
[11] H. Kazemi, K. Shinohara, G. Nagy, W. Ha, B. Lail, E. Grossman, G. Zummo, W. R. Folks, J. Alda, and G. Boreman, “First THz and IR characterization of nanometer-scaled antenna-coupled InGaAs/InP Schottky-diode detectors for room temperature infrared imaging,” *Infrared Technol. Appl. XXXIII*, vol. 6542, no. 1, 65421J, 4 pp., 2007.
[12] B. J. Eliasson, “Metal-insulator-metal diodes for solar energy conversion,” Ph.D. dissertation, Univ. Colorado, Boulder, 2001.
[13] A. Mayer, M. S. Chung, B. L. Weiss, N. M. Miskovsky, and P. H. Cutler, “Simulations of infrared and optical rectification by geometrically asymmetric metal–vacuum–metal junctions for applications in energy conversion devices,” *Nanotechnol.*, vol. 21, no. 14, 145204, 8 pp., 2010.
[14] M. Dagenais, K. Choi, F. Yesilkoy, A. N. Chryssis, and M. C. Peckerar, “Solar spectrum rectification using nano-antennas and tunneling diodes,” in *Proc. SPIE*, 2010, vol. 7605, 76050E, 11 pp.

[15] R. M. Osgood, B. R. Kimball, and J. Carlson, "Nanoantenna-coupled MIM nanodiodes for efficient vis/nir energy conversion," in *Proc. SPIE*, 2007, vol. 6652, p. 665203.
[16] B. J. Eliasson and G. Moddel, "Metal-oxide electron tunneling device for solar energy conversion" U.S. Patent 6 534 784, 2003.
[17] B. Berland, "Photovoltaic technologies beyond the horizon: Optical rectenna solar cell," Natl. Renewable Energy Lab., Golden, CO, NREL Rep. SR-520-33263, Final Rep. 2003.
[18] T. E. Hartman, "Tunneling of a wave packet," *J. Appl. Phys.*, vol. 33, no. 12, pp. 3427–3433, Dec. 1962.
[19] M. Nagae, "Response time of metal-insulator-metal tunnel junctions," *Jpn. J. Appl. Phys.*, vol. 11, no. 11, pp. 1611–1621, Nov. 1972.
[20] S. Rockwell, D. Lim, B. A. Bosco, J. H. Baker, B. Eliasson, K. Forsyth, and M. Cromar, "Characterization and modeling of metal/double-insulator/metal diodes for millimeter wave wireless receiver applications," in *Proc. IEEE Radio Frequency Integr. Circuits Symp.*, 2007, pp. 171–174.
[21] A. Sanchez, C. F. Davis, K. C. Liu, and A. Javan, "The MOM tunneling diode: Theoretical estimate of its performance at microwave and infrared frequencies," *J. Appl. Phys.*, vol. 49, no. 10, pp. 5270–5277, 1978.
[22] S. Grover, O. Dmitriyeva, M. J. Estes, and G. Moddel, "Traveling-wave metal/insulator/metal diodes for improved infrared bandwidth and efficiency of antenna-coupled rectifiers," *IEEE Trans. Nanotechnol.*, vol. 9, no. 6, pp. 716–722, Nov. 2010.
[23] M. Sarehraz, K. Buckle, T. Weller, E. Stefanakos, S. Bhansali, Y. Goswami, and S. Krishnan, "Rectenna developments for solar energy collection," in *Conf. Rec. 31st IEEE Photovoltaic Spec. Conf.*, 2005, pp. 78–81.
[24] F. J. González and G. D. Boreman, "Comparison of dipole, bowtie, spiral and log-periodic IR antennas," *Infrared Phys. Technol.*, vol. 46, no. 5, pp. 418–428, 2005.
[25] M. Sarehraz, "Novel rectenna for collection of infrared and visible radiation," Ph.D. dissertation, Univ. South Florida, Tampa, FL, 2005.
[26] J. G. Simmons, "Potential barriers and emission-limited current flow between closely spaced parallel metal electrodes," *J. Appl. Phys.*, vol. 35, no. 8, pp. 2472–2481, 1964.
[27] J. W. Dees, "Detection and harmonic generation in the submillimeter wavelength region," *Microw. J.*, vol. 9, pp. 48–55, Sep. 1966.
[28] E. W. Cowell, N. Alimardani, C. C. Knutson, J. F. Conley, D. A. Keszler, B. J. Gibbons, and J. F. Wager, "Advancing MIM electronics: Amorphous metal electrodes," *Adv. Mater.*, vol. 23, no. 1, pp. 74–78, 2011.
[29] J. R. Tucker and M. F. Millea, "Photon detection in nonlinear tunneling devices," *Appl. Phys. Lett.*, vol. 33, no. 7, pp. 611–613, Oct. 1978.
[30] J. A. Bean, B. Tiwari, G. H. Bernstein, P. Fay, and W. Porod, "Thermal infrared detection using dipole antenna-coupled metal-oxide-metal diodes," *J. Vac. Sci. Technol. B*, vol. 27, no. 1, pp. 11–14, 2009.
[31] J. A. Bean, A. Weeks, and G. D. Boreman, "Performance optimization of antenna-coupled Al/AlOx/Pt tunnel diode infrared detectors," *IEEE J. Quantum Electron.*, vol. 47, no. 1, pp. 126–135, Jan 2011.
[32] S. Grover, "Diodes for optical rectennas," Ph.D. dissertation, Univ. Colorado, Boulder, CO, 2011.
[33] G. Moddel and B. J. Eliasson, "High speed electron tunneling device and applications," U.S. Patent 6 756 649, 2004.
[34] Y. Matsumoto, T. Hanajiri, T. Toyabe, and T. Sugano, "Single electron device with asymmetric tunnel barriers," *Jpn. J. Appl. Phys.*, vol. 35, pp. 1126–1131, 1996.
[35] P. K. Tien and J. P. Gordon, "Multiphoton process observed in the interaction of microwave fields with the tunneling between superconductor films," *Phys. Rev.*, vol. 129, no. 2, pp. 647–651, Jan. 1963.
[36] J. R. Tucker and M. J. Feldman, "Quantum detection at millimeter wavelengths," *Rev. Mod. Phys.*, vol. 57, no. 4, pp. 1055–1113, Oct. 1985.
[37] P. T. Landsberg and G. Tonge, "Thermodynamics of the conversion of diluted radiation," *J. Phys. A: Math. Gen.*, vol. 12, no. 4, pp. 551–562, 1979.
[38] C. Fumeaux, W. Herrmann, F. K. Kneubühl, and H. Rothuizen, "Nanometer thin-film Ni-NiO-Ni diodes for detection and mixing of 30 THz radiation," *Infrared Phys. Technol.*, vol. 39, no. 3, pp. 123–183, 1998.
[39] I. Wilke, Y. Oppliger, W. Herrmann, and F. K. Kneubühl, "Nanometer thin-film Ni-NiO-Ni diodes for 30 THz radiation," *Appl. Phys. A: Mater. Sci. Process.*, vol. 58, no. 4, pp. 329–341, Apr. 1994.
[40] P. C. Hobbs, R. B. Laibowitz, F. R. Libsch, N. C. LaBianca, and P. P. Chiniwalla, "Efficient waveguide-integrated tunnel junction detectors at 1.6 μm," *Opt. Exp.*, vol. 15, no. 25, pp. 16376–16389, 2007.
[41] M. J. Estes and G. Moddel, "Surface plasmon devices," U.S. Patent 7 010 183, 2006.

Sachit Grover (S'03) received the B.Tech. degree in electrical engineering from the Indian Institute of Technology, New Delhi, India, in 2006 and the M.S. and Ph.D. degrees in electrical engineering from the University of Colorado at Boulder, in 2009 and 2011, respectively.

During his doctorate, he was involved in the development and analysis of high-speed diodes for antenna-coupled rectifiers that operate at optical frequencies. Currently, he is a Postdoctoral Researcher with the National Renewable Energy Laboratory, Golden, CO, working on film-silicon solar cells.

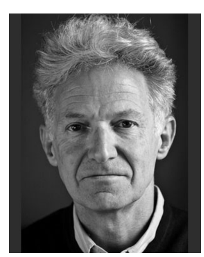

Garret Moddel (SM'93) received the B.S.E.E. degree from Stanford University, Stanford, CA, in 1976 and the M.S. and Ph.D. degrees in applied physics from Harvard University, Cambridge, MA, in 1978 and 1981, respectively.

After graduate school, he joined SERA Solar Corporation as a Founding Employee. In 1985, he joined the University of Colorado, Boulder, where he is currently a Professor with the Department of Electrical, Computer, and Energy Engineering. As a Professor, he has done research on thin-film optoelectronic materials and devices. He was the founding President and Chief Executive Officer of Phiar Corporation, which was started in 2001 to develop ultra-high-speed metal-insulator electronics. His current research interests include quantum engineering of new thin-film metal devices for energy conversion and detection.